ADVANCED FUNCTIONAL MATERIALS
www.afm-journal.de

Particle Accretion Mechanism Underlies Biological Crystal Growth from an Amorphous Precursor Phase

*Assaf Gal, Keren Kahil, Netta Vidavsky, Ross T. DeVol, Pupa U. P. A. Gilbert, Peter Fratzl, Steve Weiner, and Lia Addadi**

Many biogenic minerals are composed of aggregated particles at the nanoscale. These minerals usually form through the transformation of amorphous precursors into single crystals inside a privileged space controlled by the organism. Here, in vitro experiments aimed at understanding the factors responsible for producing such single crystals with aggregated particle texture are presented. Crystallization is achieved by a two-step reaction in which amorphous calcium carbonate (ACC) is first precipitated and then transformed into calcite in small volumes of water and in the presence of additives. The additives used are gel-forming molecules, phosphate ions, and the organic extract from sea urchin embryonic spicules - all are present in various biogenic crystals that grow via the transformation of ACC. Remarkably, this procedure yields faceted single-crystals of calcite that maintain the nanoparticle texture. The crystals grow predominantly by the accretion of ACC nanoparticles, which subsequently crystallize. Gels and phosphate ions stabilize ACC via a different mechanism than sea urchin spicule macromolecules. It is concluded that the unique nanoparticle texture of biogenic minerals results from formation pathways that may differ from one another, but given the appropriate precursor and micro-environment, share a common particle accretion mechanism.

1. Introduction

Organisms are capable of forming highly ordered crystals with shapes, sizes, and composition unequaled by synthetic counterparts.[1] It is well recognized that many organisms do not form their crystals directly from a saturated solution, but first produce a highly disordered precursor phase, from which the mature crystals are subsequently formed.[2–4] In addition, one of the most unusual hallmarks of many biogenic minerals, both amorphous and crystalline, is that at the nanoscale they are composed of spherical particles a few tens of nanometers in diameter (**Figure 1**).[5–12] This nano-particulate texture is different from the generally smooth surface of inorganic crystals at this length scale. We show here that these two observations are related.

Recent reports, in part inspired by biogenic minerals, established the existence of transient dense liquid intermediate phases as well as nanometer-sized solid clusters during mineral formation from solutions in vitro and in silico.[13–20] These studies focused on the initial nucleating phase in solution. Investigations of later stages of aggregation of disordered phases in solution showed that they can subsequently crystallize upon contact with their crystalline counterparts.[21] Moreover, at the micrometer scale some crystals appear to be meso-crystalline assemblies of nanoparticles.[22,23] Amorphous calcium carbonate (ACC) and its transformation into crystalline phases is a well-studied system because of its abundance in nature as a precursor phase and subsequent implications for synthetic systems.[24–26] Yet, despite these advances in our understanding of crystal growth processes, the phases and mechanisms that lead to the common nanoparticle morphology of biogenic minerals are unclear.[27]

Recently, we reported on a unique mode of transformation in vitro of plant cystoliths, a biogenic ACC phase that is stable as long as the leaf lives.[28] Cystoliths are found in specialized cells in the leaves of certain species of higher plants and function as light scatterers inside the leaf.[29] The ACC phase is relatively free of ionic additives, but does contain a gel-forming organic matrix.[28] Other mineralized tissues are also known to contain gel-forming molecules.[30–32] When cystoliths are induced to crystallize in vitro in a small volume of water, the cystolith ACC transforms into calcite crystals. These crystals exhibit smooth cleavage planes in their cores and nanoparticle morphology in their peripheries. We surmised that the mechanism of calcite crystal growth was initially an ion-by-ion process and then growth proceeded by ACC nanoparticle accretion and subsequent crystallization.[28] The system, however, was

A. Gal, K. Kahil, N. Vidavsky,
Prof. S. Weiner, Prof. L. Addadi
Dept. of Structural Biology
Weizmann Institute of Science
Rehovot 76100, Israel
E-mail: lia.addadi@weizmann.ac.il
R. T. DeVol, Prof. P. U. P. A. Gilbert
Dept. of Physics
University of Wisconsin-Madison
1150 University Avenue
Madison, WI 53706, USA
Prof. P. U. P. A. Gilbert
Dept. of Chemistry
University of Wisconsin-Madison
1101 University Avenue
Madison, WI 53706, USA
Prof. P. Fratzl
Dept. of Biomaterials
Max Planck Institute of Colloids and Interfaces
14424 Potsdam, Germany

DOI: 10.1002/adfm.201400676

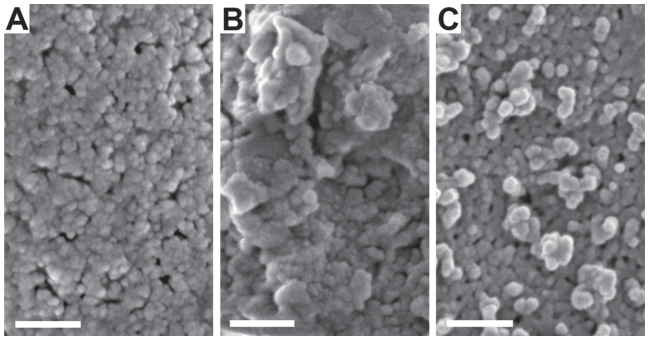

Figure 1. SEM images of the nanoscale morphology of biogenic calcium carbonate minerals. A) Surface of the sea urchin embryonic spicule extracted from a *Paracentrotus lividus* embryo 48 h after fertilization; B) surface of a fractured shell of the barnacle *Balanus amphitrite*; C) surface of a cystolith extracted from *Ficus microcarpa* leaves. Note that (A) and (B) are crystalline calcitic minerals whereas in (C) the mineral is ACC. Scale bars are 200 nm.

too complex to determine the mechanisms involved. Here, we report the results of in vitro experiments in which calcite crystals are formed from synthetic disordered precursor phases in several different environments, and these crystals exhibit the surface and bulk nanoparticle texture of many biogenic crystals.

2. Results

We investigated the influence of three different biologically relevant additives on the transformation of synthetic ACC into calcite: gel-forming molecules, phosphate ions, and an extract of macromolecules from sea urchin spicules. The gel-forming molecules tested are: pectin, which is present in the cystolith organic fraction[28] and comprises a family of polysaccharides where galacturonic acid is dominant; agarose, a neutral polysaccharide; and gelatin, denatured and partially hydrolyzed collagen. Phosphate ions are common in biogenic ACC phases[33] and are known to stabilize biogenic ACC.[34] Phosphate is an inhibitor of calcite crystal growth and calcite dissolution, and slows the kinetics of these processes.[35] The third type of additive used is an extract of the organic molecules embedded in the embryonic spicules of the sea urchin *Paracentrotus lividus* (referred to as spicule extract). These macromolecules, predominantly proteins, are known to induce and stabilize the formation of transient ACC precursor phases in vitro.[36,37]

Each additive was tested in two experimental procedures differing in the manner in which the additive is introduced. Procedure (i): ACC was precipitated by mixing and immediately drying solutions containing calcium, carbonate, and the additive. In the case of gel-forming molecules the solutions were maintained at ≈40 °C, which is above the gelation temperature, until mixing. The other preparations were done at room temperature. This reaction yielded dry powder consisting of ACC intermixed with additive molecules (Figure S1, Supporting Information), and was used as the starting material for the transformation reaction. The additive-containing ACC was transformed into calcite by immersion in double distilled water (DDW). Procedure (ii): ACC was precipitated without an additive and was used as the starting material for the transformation reaction. The transformation took place inside a solution containing the additive in the case of phosphate ions and the spicule extract, or inside a gel in the case of the gel-forming molecules. As a control, ACC was transformed in DDW in the absence of any additive. In all experiments 3 mg of ACC were transformed in 200 µl of solution or gel for two hours. Before crystallization, all ACC samples were composed of porous aggregates of spherical nanoparticles 15–50 nm in size (Figure S2, Supporting Information).

2.1. Morphological Characterization of Transformed ACC Samples

Fourier transform infrared (FTIR) spectroscopy shows that the ACC transformed into a mixture of calcite and vaterite in all cases except for the sea urchin extract where only calcite formed (**Table 1** and Figure S3, Supporting Information). Accordingly, scanning electron microscope (SEM) images show characteristic calcite crystals expressing their most stable rhombohedral faces, as well as globular aggregates of vaterite crystals (Figure S4, Supporting Information).

The presence of the gel-forming molecules, either co-precipitated with ACC or introduced through the aqueous environment, causes a major change in the calcite nanoscale morphology. Whereas at the micrometer scale the crystals show the stable {104} faces of calcite rhombohedra, at the nanoscale the rhombohedral surfaces consist of an aggregation of nanoparticles, reminiscent of the ACC nanoparticles before transformation (**Figure 2**A–C, Figure S5, Supporting Information). The smooth nano-scale morphology of the crystals formed from additive-free ACC is in sharp contrast to the nano-scale morphology of the crystals that grew in the presence of the gels (Figure 2D). Fracturing the crystals shows that the nanoparticle morphology characterizes also the inner bulk (Figure 2F and Figure S6, Supporting Information). Clearly, the gel phase is responsible for the formation of calcite crystals with nanoparticles on the surface and the interior. The type of gel does not appear to be important.

In order to investigate the local environment of the crystal growth process, the transformation of gelatin-containing ACC

Table 1. Mineralogy of the crystals resulting from the transformation of ACC in the presence of additives.

Additive	Procedure (i)		Procedure (ii)	
	%Calcite[a)]	%Vaterite[a)]	%Calcite[a)]	%Vaterite[a)]
Pectin	25	75	50	50
Agarose	75	25	N/D[b)]	
Gelatin	65	35	50	50
PO_4^{3-}	85	15	60	40
Spicule extract	100	0	30	70
None	N/A		30	70

[a)]The phase composition was determined using a calibrated area ratio of the $\nu 4$ peaks of calcite and vaterite in the FTIR spectrum of the bulk material (Figure S3, Supporting Information). The experimental variance between different batches is 5%; [b)]The extraction of the crystals from the agarose gel involves heating to temperatures that might affect the phase composition (see Experimental Section).

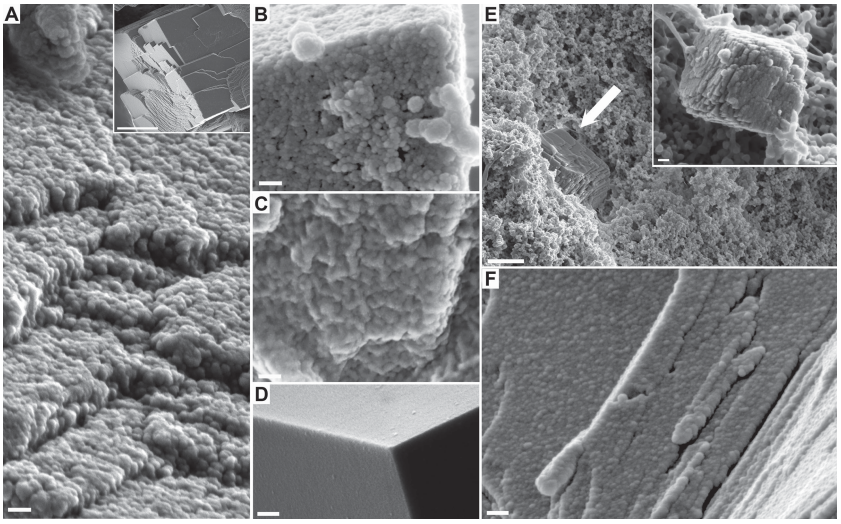

Figure 2. SEM images of calcite crystal surfaces resulting from procedure (ii): the transformation of ACC in A) gelatin gel (inset shows a low magnification image of a crystal), B) pectin gel, C) agarose gel, and D) with no additive. E) Calcite crystallite (indicated by an arrow) surrounded by ACC nanoparticles that formed after 1 min of transformation from gelatin containing ACC (procedure (i)). The inset shows a high magnification image of such a crystallite. F) Fracture surface inside a crystal that was grown by the transformation of gelatin-containing ACC (procedure (i)) and mechanically fractured to expose the interior texture. Similar fracture surfaces were also observed inside crystals resulting from transformations in the presence of all additives (Figure S6, Supporting Information). Scale bars are 100 nm; 10 μm for the inset in A, except for panel E where the scale bar is 1 μm and 100 nm for the inset.

was quenched after one minute by replacing DDW with ethanol. At this stage only a small fraction of the ACC had crystallized (Figure 2E). Sub-micron crystals develop inside the dense ACC bulk such that the distance from the crystal surface to the ACC particles is less than a micrometer. These crystallites show a rough morphology, characterized by well-defined rhombohedral facets at the sub-micron scale (Figure 2E inset).

The influence of the second type of additive, phosphate ions, either inside the ACC or in the solution, is similar to that of the gels (**Figure 3** and Figure S5, Supporting Information). The higher the phosphate concentration, the more dominant is the nanoparticle morphology on the crystal faces.

With the sea urchin spicule macromolecules the crystals also grow by the nanosphere accretion process, resulting in a nanometer scale appearance remarkably similar to the biogenic spicules. In contrast to the previous cases, the effect is more pronounced when ACC is co-precipitated with the macromolecules, whereas it is marginal when the macromolecules are present only in the solution (**Figure 4**). Note that vaterite was absent only in the synthetic experiments in which the spicule extract co-precipitated with ACC (Table 1). This indicates that the spicule extract also exerts control over the crystal nucleation step.

2.2. X-PEEM Analysis of Untransformed and Transformed ACC Samples

X-ray photoemission electron microscopy (X-PEEM) was previously used to show that ACC particles persist for days inside the forming sea urchin embryonic spicule and that the mature spicule is not composed uniformly of calcite, but has interspersed islands of the precursor ACC phases.[37,38] We therefore used X-PEEM at the Ca L-edge to determine if the freshly formed calcite crystals grown in the presence of the spicule extract have similar properties. Cross-sections of extract-containing ACC samples, before and after transformation in water, were analyzed with 20 nm resolution using X-PEEM.[39] Even though the initial amorphous phase was immersed in water for only 15 min to minimize the transformation time, and the analysis was carried out shortly after the transformation, the entire crystal was composed of calcite (**Figure 5**). Therefore, no detectable islands of ACC were preserved inside the growing crystal, unlike the situation in the biogenic spicule, which grows without a direct contact with water.[40]

2.3. XRD Analysis of Transformed ACC Samples

We used single-crystal X-ray diffraction (XRD) to qualitatively examine the crystal texture of the crystals exhibiting a nanoparticle morphology. The diffraction patterns of isolated crystals resulting from transformations in the presence of the different additives consist of sharp spots that indicate their single-crystalline nature (Figure S7, Supporting Information). In addition, the crystalline properties of the crystals resulting from the transformation of ACC containing the spicule extract were quantitatively characterized using high-resolution synchrotron-based micro-XRD (**Figure 6**). Analysis of the {104} diffraction peaks from 20 crystals yielded, according to the Scherrer equation, a minimal coherence length (the average size of perfect lattice domains) of 150 nm.[41] Since the determination of coherence lengths is limited by the experimental resolution, the actual coherence length of the crystals may be much larger than 150 nm. Analogously, possible contributions of lattice strain, which result in broadening of the diffraction peaks, cannot be detected because they are below the instrumental detection limit.[42] Not only does the extended lattice order show the high crystallinity typical of calcite single crystals, it also shows that the average length of perfect lattice

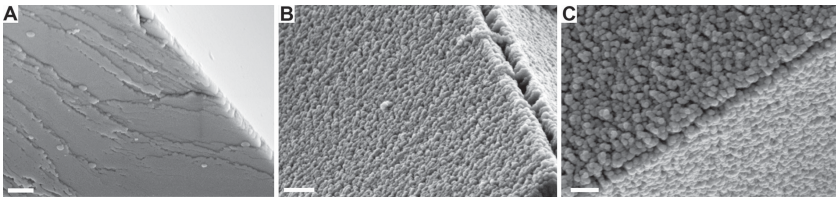

Figure 3. SEM images of calcite crystal surfaces resulting from the transformation of ACC in solution containing A) 0.1 mM PO_4^{3-}, B) 1 mM PO_4^{3-}, and C) 10 mM PO_4^{3-} (procedure (ii)). Scale bars are 200 nm.

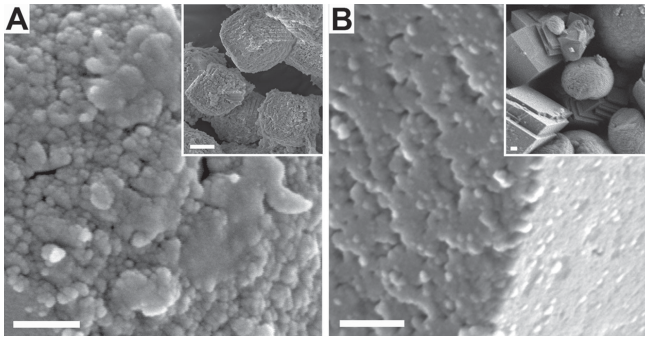

Figure 4. SEM images of A) the surface of a single crystal of calcite resulting from the transformation of ACC containing the organic extract of sea urchin spicules in DDW (procedure (i)) and B) the surface of a calcite crystal resulting from the transformation of ACC in solution containing the organic extract of sea urchin spicules (procedure (ii)). Note faces and steps at the nm scale. Insets show lower magnification images. Scale bars are 100 nm, and 1 μm for the insets.

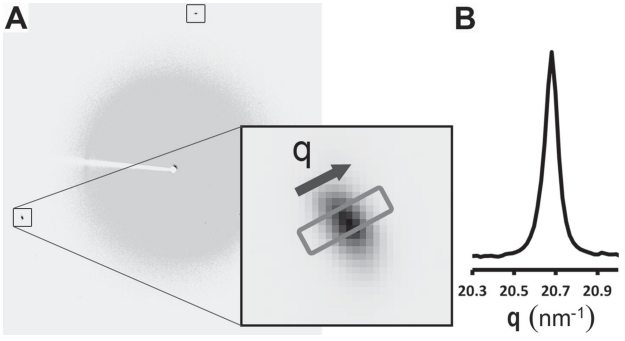

Figure 6. A) High resolution micro-XRD pattern collected from a single crystal of calcite resulting from the transformation of ACC containing the sea urchin spicule extract in DDW (procedure (i)). Rectangles indicate the two sharp {104} diffraction spots. One spot is magnified in the inset and the area used for the radial integration is shown. B) Radially integrated profile of the magnified diffraction peak in (A). The peak widths at half maximum from different crystals were used in the coherence length analysis.

domains, presumably interrupted by the occluded macromolecules, proceeds through at least 5 nanoparticles. Note that lattice imperfections, which are conceivably concentrated at the surface of the particles, will guide the propagation of fracture planes, thus evidentiating the nanoparticle morphology. However, these imperfections do not appear to completely envelope the nanoparticles, allowing lattice continuity to extend from one particle to the next, thus accounting for the extended coherence length.

2.4. Thermal Stability of ACC Samples

We measured the thermal stability of the ACC samples used in the experiments in order to determine the relative stabilities of the different ACC phases and to test the role of thermodynamic stabilization in the process. ACC samples co-precipitated with each of the tested additives as well as additive-free ACC were heated to elevated temperatures for an hour, and after cooling were analyzed with FTIR spectroscopy to determine if crystallization occurred. All the ACC samples crystallized into calcite after heating to 280–300 °C, except for the ACC containing spicule extract which started to crystallize after heating to 260 °C (Figure S8, Supporting Information). This range of crystallization temperatures is in agreement with previous studies of the thermal stability of synthetic ACC.[43] Therefore, no additive-containing ACC is thermally more stable than the additive-free ACC. In the phosphate case, additional experiments with higher phosphate concentrations showed that this is because the amount of phosphate ions in our experiments is too low to have a detectable effect (Figure S8, Supporting Information). In the case of the organic additives, the molecules are at least partially charred during heating (Figure S1, Supporting Information), in which case a thermodynamic influence of the additives on the ACC stability is not detectable using this method.

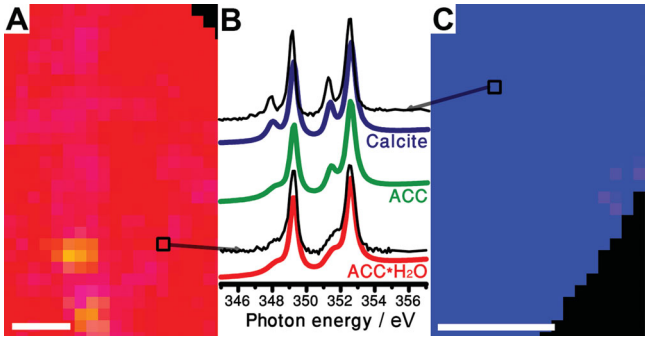

Figure 5. XPEEM Ca L-edge component analysis maps of: A) synthetic ACC co-precipitated with the sea urchin spicule extract (20 nm pixels); and C) a calcite crystal that resulted from the transformation of this extract-containing ACC (procedure (i), 10 nm pixels). A linear combination of the 3 reference spectra of hydrous ACC, anhydrous ACC, and calcite (shown in panel B with their color code) was used to fit the XANES spectrum extracted from each 10 or 20 nm pixel.[34] The pixels on the maps are colored according to the relative intensity of each component and the RGB mixing rule. The ACC map is mostly red as it is mainly composed of un-transformed hydrated ACC. The nearly homogenous blue color in (C) indicates the lack of any phases other than calcite. Two representative spectra taken from the single pixels indicated in the panels A and C are presented in black in panel B. Scale bars are 100 nm.

3. Discussion

The ACC-to-calcite transformations described here share common features with biogenic systems. In both synthetic and biological systems, crystal formation is a two-step process, where the initial formation of ACC is followed by the transformation of this phase into calcite crystals. This two-step reaction in our in vitro experiments also allows for the second step of ACC transformation to occur in sub-micron proximity to the bulk ACC phase (Figure 2E). Under these conditions the ACC nanoparticles can be stabilized by additives such that they undergo short-range migration and crystallization on the growing crystal.

The driving force for the ACC-to-calcite transformation is the thermodynamic stability of the crystalline phase, which is reflected in the higher solubility of the amorphous phase. Kinetically, in the absence of additives, the dominant process is ACC dissolution into ions and subsequent ion-by-ion crystal

growth. The presence of the additives changes the nature of the transformation process to a particle accretion mechanism in a gradual manner, depending on the additive concentration. In the case of gels and phosphate ions this change is essentially a kinetic effect. This is deduced from the observation that it does not matter if the additive is present in the solution or co-precipitated within the ACC phase. Moreover, in the case of phosphate ions the concentration needed to induce the accretion process is so low that no change in the thermal stability of ACC is detected.

The evidence in favor of a kinetics-dominated process is further supported by the accepted role of additives as kinetic inhibitors of ion-by-ion crystal growth and dissolution. Specifically, interactions of gels with water molecules,[32,44] or interactions of phosphate ions with crystal surfaces,[45,46] were shown to kinetically slow down the ion-mediated processes. The gel induces confinement of the solution into delimited volumes. Such confined volumes were shown to stabilize ACC.[47] We suggest that by slowing down the ion-mediated process, the additives change the kinetic balance between the two competing crystal growth processes such that the particle-mediated process dominates.

On the other hand, the sea urchin spicule extract is effective predominantly when the macromolecules are present inside the initial ACC phase, and their molar concentration is 2–5 orders of magnitude lower than that of the other additives. This suggests that the biogenic macromolecules stabilize the ACC phase against dissolution by chemical interactions in the bulk of the ACC, thus changing the transformation process. This effect, which is different from that of the other additives, might originate from a different kinetic pathway or from altering the thermodynamic stability of the material.

The in vitro crystallization pathway induced by the spicule extract closely reproduces the texture of the biogenic minerals. However, the synthetic crystals show crystallographic habit and lack traces of ACC; both properties differ from the biogenic spicule formation process. This is conceivably the result of the different environments of the reactions. In vivo, the transformation occurs inside confined chambers, with the crystal adopting the shape of the chamber, and no bulk water phase is detected.[48] In the synthetic experiments the local presence of bulk water enables migration of a particle to an energetically favorable site before crystallization. In contrast to the biogenic environment, the particle mobility in the synthetic experiments makes it less likely for an amorphous particle to be trapped in the crystal and to persist as an amorphous island, such as was observed in the formed sea urchin embryonic spicule.[37]

It is counter intuitive that the particle accretion process, involving aggregation of spherical amorphous particles, results in crystals displaying the most thermodynamically stable {104} faces of calcite. The development of crystal faces is normally the result of different attachment kinetics of ions to different crystal planes due to anisotropic attachment energies.[49,50] These faces have the highest ion density, are balanced with respect to positive and negative charges, and thus are the most stable. The formation of rough crystal faces composed of aggregated particles suggests that anisotropic forces, similar to the ion-mediated process, control the site at which a nanoparticle stops migrating on the crystal surface, fuses with the crystal, and after crystallization becomes part of the lattice. This can be

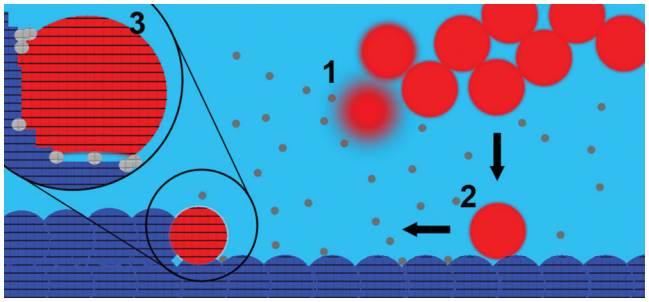

Figure 7. Crystal growth pathways. 1) Upon immersion of ACC (red) in water, the ACC particles can undergo partial dissolution (blurred particles) into ions (gray). This process of ACC dissolution into ions, as well as the process of ion-by-ion crystal growth, is slowed down by the presence of additives. (2) An ACC particle can migrate to the crystal surface (blue) where diffusion and surface tension will favor its movement towards steps and kinks on the crystal surface. (3) Particle crystallization at such preferred sites will be favored, whereby they will become integral parts of the crystal. Ion-by-ion attachment to the crystal is occurring concomitantly with particle accretion.

rationalized as follows (**Figure 7**): the habit of the initial crystallite is rhombohedral (Figure 2E), because it originates from an ion-mediated nucleation step. The ACC particles stabilized by the additive can resist dissolution for an extended amount of time and migrate to the crystallite surface. On the rhombohedral crystal surface, diffusion and surface tension will favor the migration of particles to kinks or steps. In these locations the particle interacts with the crystal over an extended area, thus favoring crystallization. In addition, the aqueous environment may facilitate reconstruction of the spherical particles into faceted particles by local dissolution-reprecipitation. This, together with concomitant ion-by-ion growth, results in crystal surfaces that are composed of {104} faces at a close-to-atomic scale. Lastly, when sea urchin embryos, characterized by spicules with convoluted curved surfaces, were grown in low Mg and Ca concentrations or in the presence of other ions, the spicules grew anomalously and showed {104} faces with rough nanostructured surfaces.[51] This might imply that disturbed biological control yields the default rhombohedral habit also in vivo.

The properties of the synthetic calcite crystals grown from ACC containing the spicule macromolecules provide a solution to long-standing apparent contradictions arising from the biogenic process. Firstly, even though the nanoparticle morphology and the lack of crystallographic habit of the spicule suggest a solid-state amorphous-to-crystalline transition, the organic components of the spicule are anisotropically dispersed inside the mineral, preferentially residing along {100} planes.[52] This textural anisotropy is conventionally associated with adsorption processes driven by molecular recognition occurring in bulk solution.[53] Secondly, the macromolecules are thought to be homogenously distributed in the ≈20 nm ACC particles and to stabilize them. However, in the crystalline spicule the average distance between lattice imperfections as determined by the coherence length of the lattice is 125 nm,[54] suggesting a nanometer-scale rearrangement of the embedded proteins which is hard to conceive in a solid-state reaction.

Our experiments show that the aqueous particle accretion process is compatible with these two properties of biogenic

crystals. Water is present in the transformation process even though dissolution does not dominate, and its presence may explain the observed phenomena. The initial ACC phases in both the biogenic and synthetic cases are hydrated phases, where the water molecules were suggested to concentrate in nanometer-sized channels.[17,55] Therefore, water elimination from the ACC before crystallization can have a major effect on its properties and the expelled water may be sufficient to provide a nanoscale solution environment. In vivo, this eliminated water may facilitate local aqueous interactions between crystal surfaces and additives as well as long range rearrangement of imperfections in the lattice.[56] Nanoconfined water channels can thus explain the anisotropic intercalation of additives in the biogenic crystals, while the lack of bulk water, which could favor the ion-mediated process, allows preservation of the nanoparticle morphology. This does not preclude the possibility of a solid-to-solid transformation of the anhydrous ACC phase into calcite, as detected in biogenic minerals.[37,38]

The change in crystal growth mechanism shown here, from an ion-mediated process to a particle-accretion process, demonstrates how different strategies can lead to the characteristic nanoparticle texture of biogenic minerals. Several biominerals form inside gel-like matrices with varying chemical properties,[32] and more may well be discovered. In all these systems a kinetic effect that is largely independent of the chemistry of the macromolecules can have a major impact on the crystallization pathway. Specific interactions of additives, such as inorganic ions or organic macromolecules with the amorphous and crystalline phases, can lead to kinetic and/or thermodynamic control over the crystallization pathway.

4. Conclusions

The synthetic experiments presented here show that crystallization can proceed by the attachment of nanoparticles to a growing crystal and their incorporation into the ordered lattice after crystallization. Our results show that in the case of calcium carbonate, if nanoparticles are present in solution in addition to ions, there is a kinetic competition between the attachment of the two species during crystal growth. The presence of an additive might stabilize the amorphous particles through a kinetic and/or thermodynamic effect, making them less soluble. This can change the crystallization pathway such that the particle-mediated crystal growth process dominates and the morphology of the crystal is reminiscent of aggregated particles. Many organisms form their minerals from amorphous precursors inside a privileged space in the absence of bulk water and in the presence of additives similar to the ones we used synthetically. Thus, the origin of many properties of biogenic minerals, such as their shape, crystallinity, composition, and nano-particulate texture, may originate from such a crystallization pathway.

5. Experimental Section

Additive Solutions: Powders of the gel-forming macromolecules were dissolved in hot DDW. 0.5% Pectin from apple (Sigma) solution, 0.5% SeaKem LE agarose (BMA) solution, and 5% gelatin type B from bovine skin 75 Bloom (Sigma) solution were used. These concentrations, which are above the critical concentration for the formation of a gel, were the highest that would enable mixing of ≈40 °C liquid phase solutions and drying of the precipitate. With higher concentrations it was impossible to isolate an amorphous precipitate, and with lower concentrations the accretion process was less dominant. Na_3PO_4 (Sigma) solution at the appropriate concentration was used as the phosphate additive. Embryos of the sea urchin *Paracentrotus lividus* were grown for about 48 h. At this stage the spicules were extracted according to well-established protocols.[36] The spicules were demineralized by immersing in DDW and a drop-wise addition of a calculated volume of 0.1 M HCl.[54] The protein concentration used (35 nmol ml^{-1}) is the same as in previous experiments performed to study the macromolecule effect on crystallization,[36] and was calculated according to the known fraction of spicule proteins in the mineral.[57]

ACC Precipitation and Transformation: Calcium chloride and sodium carbonate solutions (reagents by Sigma) were prepared by diluting a 1 M stock solution in DDW or in an additive solution. Sodium carbonate (0.5 ml of 100 mM) was added to calcium chloride (0.5 ml of 100 mM). Immediately after mixing, the solution was filtered with a membrane filter, washed with absolute ethanol, and dried under a heating lamp. The dried precipitates were kept in a desiccator.

3 mg aliquots of the dry ACC sample were placed in 2 ml Eppendorf plastic tubes containing 200 µl of solution (DDW or an additive solution). In the case of gels, a warm liquid solution was poured over the ACC and immediately cooled to induce gelation. The tubes were left closed at ambient temperature for 2 h. After that the solution was washed once with DDW and twice with ethanol and then dried. In the case of transformation inside a gel, the gel was heated gently so it became liquid again and then washed.

SEM and FTIR Characterization: ACC and calcite samples were coated with chromium and imaged using an ULTRA 55 scanning electron microscope (Zeiss). Each calcite sample was fractured by gentle crushing with an agate mortar and pestle and the interior surfaces were examined. For FTIR spectroscopy the sample was ground, embedded in a KBr pellet, and measured with a NICOLET iS5 spectrometer. For heating experiments the samples were placed for 1 h in an oven preheated to the desired temperature.

X-PEEM: ACC and calcite samples were embedded in epoxy (Epofix, EMS, Hatfield, PA, USA), polished to expose cross-sections, coated (sputter coater 208HR, Cressington, UK) with 1 nm Pt in the area to be analyzed by XANES-PEEM, and covered with 40 nm Pt around it. They were then analyzed with PEEM-3 on beamline 11.0.1 at the Advanced Light Source - Berkeley.[39] A stack of images was collected across the Ca L-edge, between photon energies of 340 and 360 eV (121 images, with field of view either 10 × 10 µm or 20 × 20 µm images, and pixel sizes 10-nm or 20-nm, respectively), with a sample voltage of 18 kV. Each pixel in a stack contained the complete Ca L-edge XANES spectrum and was fitted to a linear combination of the three component spectra of hydrated ACC, anhydrous ACC, and calcite, as described in Gong et al.[37]

XRD: In-house single crystal XRD was carried out on a Rigaku diffractometer using AU3HR generator and Raxis IV ++ detector. The samples were mounted on thin glass fibers using Paratone oil (Hampton Research). High-resolution micro-XRD measurements were carried out on beamline P03 at DESY, Hamburg.[58] Crystals were mounted on a Mylar (DuPont) tape and measured using a 1 micron diameter beam at 15 keV. The acquisition time was 0.5 s and the sample-detector distance was 281.9 mm, as determined using an LaB_6 standard. Under these conditions the theoretical resolution of the measurement at $q = 20.7$ nm^{-1} is 0.080 nm^{-1}, the measured widths of the calcite {104} peaks were 0.075 ± 0.012 nm^{-1}.

Supporting Information

Supporting Information is available from the Wiley Online Library or from the author.

Acknowledgements

The authors thank L. J. W. Shimon, W. Wagermaier, M. Kerschnitzki, and A. Akiva for their help with the XRD measurements. The research was supported by a German Research Foundation grant within the framework of the Deutsch–Israelische Projektkooperation, by a Department of Energy award (DE-FG02-07ER15899), and National Science Foundation award DMR-1105167. The Advanced Light Source is supported by the Department of Energy award DE-AC02-05CH11231. L.A. is the incumbent of the Dorothy and Patrick Gorman Professorial Chair of Biological Ultrastructure, and S.W. of the Dr. Trude Burchardt Professorial Chair of Structural Biology.

Received: February 27, 2014
Revised: April 17, 2014
Published online: July 1, 2014

[1] H. A. Lowenstam, S. Weiner, *On Biomineralization*, Oxford University Press, New York **1989**.
[2] E. Beniash, J. Aizenberg, L. Addadi, S. Weiner, *Proc. R. Soc. London Ser. B* **1997**, *264*, 461.
[3] S. Raz, P. C. Hamilton, F. H. Wilt, S. Weiner, L. Addadi, *Adv. Funct. Mater.* **2003**, *13*, 480.
[4] J. Mahamid, A. Sharir, L. Addadi, S. Weiner, *Proc. Natl. Acad. Sci. USA* **2008**, *105*, 12748.
[5] Y. Dauphin, *Paläontologische Zeitschrift* **2001**, *75*, 113.
[6] X. D. Li, W. C. Chang, Y. J. Chao, R. Z. Wang, M. Chang, *Nano Letters* **2004**, *4*, 613.
[7] Y. Oaki, H. Imai, *Small* **2006**, *2*, 66.
[8] N. Watabe, D. G. Sharp, K. M. Wilbur, *J. Biophys. Biochem. Cytol.* **1958**, *4*, 281.
[9] Y. Isa, *Mar. Biol.* **1986**, *93*, 91.
[10] J. P. Cuif, Y. Dauphin, *J. Struct. Biol.* **2005**, *150*, 319.
[11] M. Cusack, Y. Dauphin, P. Chung, A. Perez-Huerta, J. P. Cuif, *J. Struct. Biol.* **2008**, *164*, 96.
[12] D. E. Jacob, A. L. Soldati, R. Wirth, J. Huth, U. Wehrmeister, W. Hofmeister, *Geochim. Cosmochim. Ac.* **2008**, *72*, 5401.
[13] D. Gebauer, A. Volkel, H. Colfen, *Science* **2008**, *322*, 1819.
[14] E. M. Pouget, P. H. H. Bomans, J. A. C. M. Goos, P. M. Frederik, G. de With, N. A. J. M. Sommerdijk, *Science* **2009**, *323*, 1455.
[15] L. B. Gower, D. J. Odom, *J. Cryst. Growth* **2000**, *210*, 719.
[16] A. F. Wallace, L. O. Hedges, A. Fernandez-Martinez, P. Raiteri, J. D. Gale, G. A. Waychunas, S. Whitelam, J. F. Banfield, J. J. De Yoreo, *Science* **2013**, *341*, 885.
[17] P. Raiteri, J. D. Gale, *J. Am. Chem. Soc.* **2010**, *132*, 17623.
[18] E. D. Eanes, I. H. Gillessen, A. S. Posner, *Nature* **1965**, *208*, 365.
[19] L. J. Wang, G. H. Nancollas, *Chem. Rev.* **2008**, *108*, 4628.
[20] W. J. E. M. Habraken, J. H. Tao, L. J. Brylka, H. Friedrich, L. Bertinetti, A. S. Schenk, A. Verch, V. Dmitrovic, P. H. H. Bomans, P. M. Frederik, J. Laven, P. van der Schoot, B. Aichmayer, G. de With, J. J. DeYoreo, N. A. J. M. Sommerdijk, *Nat. Commun.* **2013**, 4.
[21] J. Baumgartner, A. Dey, P. H. H. Bomans, C. Le Coadou, P. Fratzl, N. A. J. M. Sommerdijk, D. Faivre, *Nat. Mater.* **2013**, *12*, 310.
[22] H. Colfen, M. Antonietti, *Angew. Chem. Int. Ed.* **2005**, *44*, 5576.
[23] R. Q. Song, H. Colfen, *Adv. Mater.* **2010**, *22*, 1301.
[24] J. Seto, Y. R. Ma, S. A. Davis, F. Meldrum, A. Gourrier, Y. Y. Kim, U. Schilde, M. Sztucki, M. Burghammer, S. Maltsev, C. Jager, H. Colfen, *Proc. Natl. Acad. Sci. USA* **2012**, *109*, 7126.
[25] C. Li, L. M. Qi, *Angew. Chem. Int. Ed.* **2008**, *47*, 2388.
[26] J. Ihli, Y. Y. Kim, E. H. Noel, F. C. Meldrum, *Adv. Funct. Mater.* **2013**, *23*, 1575.
[27] S. Weiner, L. Addadi, *Annu. Rev. Mater. Res.* **2011**, *41*, 21.
[28] A. Gal, W. Habraken, D. Gur, P. Fratzl, S. Weiner, L. Addadi, *Angew. Chem. Int. Ed.* **2013**, *52*, 4867.
[29] A. Gal, V. Brumfeld, S. Weiner, L. Addadi, D. Oron, *Adv. Mater.* **2012**, *24*, OP77.
[30] Y. Levi-Kalisman, G. Falini, L. Addadi, S. Weiner, *J. Struct. Biol.* **2001**, *135*, 8.
[31] G. M. Khalifa, S. Weiner, L. Addadi, *Cryst. Growth Des.* **2011**, *11*, 5122.
[32] E. Asenath-Smith, H. Y. Li, E. C. Keene, Z. W. Seh, L. A. Estroff, *Adv. Funct. Mater.* **2012**, *22*, 2891.
[33] A. P. Vinogradov, *The Elementary Chemical Composition of Marine Organisms*, Yale University, New Haven **1953**.
[34] A. Al-Sawalmih, C. Li, S. Siegel, P. Fratzl, O. Paris, *Adv. Mater.* **2009**, *21*, 4011.
[35] J. R. Clarkson, T. J. Price, C. J. Adams, *J. Chem. Soc. Faraday Trans.* **1992**, *88*, 243.
[36] S. Raz, P. C. Hamilton, F. H. Wilt, S. Weiner, L. Addadi, *Adv. Funct. Mater.* **2003**, *13*, 480.
[37] Y. U. T. Gong, C. E. Killian, I. C. Olson, N. P. Appathurai, A. L. Amasino, M. C. Martin, L. J. Holt, F. H. Wilt, P. U. P. A. Gilbert, *Proc. Natl. Acad. Sci. USA* **2012**, *109*, 6088.
[38] Y. Politi, R. A. Metzler, M. Abrecht, B. Gilbert, F. H. Wilt, I. Sagi, L. Addadi, S. Weiner, P. U. P. A. Gilbert, *Proc. Natl. Acad. Sci. USA* **2008**, *105*, 17362.
[39] A. Doran, M. Church, T. Miller, G. Morrison, A. T. Young, A. Scholl, *J. Electron Spectrosc. Relat. Phenom.* **2012**, *185*, 340.
[40] E. Beniash, L. Addadi, S. Weiner, *J. Struct. Biol.* **1999**, *125*, 50.
[41] A. Guinier, *X-Ray Diffraction in Crystals, Imperfect Crystals, and Amorphous Bodies*, W.H. Freeman, San Francisco, CA **1963**.
[42] B. Pokroy, A. N. Fitch, E. Zolotoyabko, *Adv. Mater.* **2006**, *18*, 2363.
[43] N. Koga, Y. Z. Nakagoe, H. Tanaka, *Thermochim. Acta* **1998**, *318*, 239.
[44] H. K. Henisch, *Crystals in Gels and Liesegang Rings*, Cambridge University Press, Cambridge **2005**.
[45] P. M. Dove, M. F. Hochella, *Geochim. Cosmochim. Ac.* **1993**, *57*, 705.
[46] J. Klasa, E. Ruiz-Agudo, L. J. Wang, C. V. Putnis, E. Valsami-Jones, M. Menneken, A. Putnis, *Geochim. Cosmochim. Ac.* **2013**, *117*, 115.
[47] C. J. Stephens, S. F. Ladden, F. C. Meldrum, H. K. Christenson, *Adv. Funct. Mater.* **2010**, *20*, 2108.
[48] F. H. Wilt, *Zool. Sci.* **2002**, *19*, 253.
[49] P. Hartman, W. G. Perdok, *Acta Crystallogr.* **1955**, *8*, 49.
[50] L. Addadi, Z. Berkovitchyellin, I. Weissbuch, J. Vanmil, L. J. W. Shimon, M. Lahav, L. Leiserowitz, *Angew. Chem. Int. Ed.* **1985**, *24*, 466.
[51] K. Okazaki, S. Inoue, *Dev. Growth Differ.* **1976**, *18*, 413.
[52] A. Berman, J. Hanson, L. Leiserowitz, T. F. Koetzle, S. Weiner, L. Addadi, *Science* **1993**, *259*, 776.
[53] S. Mann, *Biomineralization: Principles and Concepts in Bioinorganic Materials Chemistry*, Oxford University Press, New York **2001**.
[54] J. Aizenberg, J. Hanson, T. F. Koetzle, S. Weiner, L. Addadi, *J. Am. Chem. Soc.* **1997**, *119*, 881.
[55] A. L. Goodwin, F. M. Michel, B. L. Phillips, D. A. Keen, M. T. Dove, R. J. Reeder, *Chem. Mater.* **2010**, *22*, 3197.
[56] J. Aizenberg, D. A. Muller, J. L. Grazul, D. R. Hamann, *Science* **2003**, *299*, 1205.
[57] S. Weiner, *J. Exp. Zool.* **1985**, *234*, 7.
[58] A. Buffet, A. Rothkirch, R. Dohrmann, V. Korstgens, M. M. A. Kashem, J. Perlich, G. Herzog, M. Schwartzkopf, R. Gehrke, P. Muller-Buschbaum, S. V. Roth, *J. Synch. Rad.* **2012**, *19*, 647.